

Numerical and Experimental Analysis of the Influence of Projectile Impact Angle on Armour Plate Protection Capability

Dawid Pacek and Przemysław Badurowicz*

Military Institute of Armament Technology, 7 Prymasa Stefana Wyszyńskiego Street, Poland

**E-mail: badurowiczp@witu.mil.pl*

ABSTRACT

This research manuscript describes the process of degradation of an Armox 600 armour plate during the impact of a 5.56×45 mm SS109 projectile. The creation process of the numerical FEM model of the projectile is presented. The projectile impact angle is set between 15° and 90°, and this phenomenon is investigated via numerical and experimental approaches. The experiment is conducted under the same conditions as the numerical approach to validate the FEM model. The experiments are conducted using a high-speed camera. This research manuscript presents the influence of the projectile impact angle on the degradation of the armour plate and its protection capability for different angles. The results demonstrate the dependence of the transferred energy on the armour plate, speed of the particles after impact, and trace dimensions on the armour plate for different impact angles.

Keywords: Mechanics; Terminal ballistics; Finite element method; Armour plate; Projectile ricochet

NOMENCLATURE

A	: Static yield stress	T	: Temperature
B	: Strain hardening coefficient	T^*	: Homologous temperature (dimensionless value of temperature)
C	: Strain rate coefficient	T_p	: Room temperature
c_0	: Bulk speed of sound in material	T_t	: Melting temperature
D_1	: Material constant 1	u_p	: Particle velocity
D_2	: Material constant 2	u_s	: Shock velocity
D_3	: Material constant 3	V	: Volume
D_4	: Material constant 4	V_0	: Initial volume
D_5	: Material constant 5	w	: Width of a trace
d_p	: Depth of a trace	Y	: Yield stress
e	: Energy	Γ	: Gruneisen coefficient
e_H	: Internal energy per unit mass	Γ_0	: Initial Gruneisen coefficient
E_{k0}	: Initial kinetics energy – before an impact of a projectile	$\Delta\varepsilon$: Increment of the effective plastic strain
E_{kr}	: Residual kinetics energy – after an impact of a projectile	ε	: Equivalent plastic strain
E_T	: Energy transferred into the armour plate	$\dot{\varepsilon}^*$: Dimensionless plastic strain rate
h	: Height of a trace	ε_0	: Reference rate of plastic deformation
G	: Shear modulus	ε_f	: Equivalent plastic strain at failure
K	: Bulk modulus	ρ	: Density due to shock compression
m	: Thermal softening exponent	ρ_0	: Initial density
n	: Strain hardening exponent	σ	: Yield stress
p	: Pressure	σ^*	: Pressure/stress measureless dependence
p_0	: Initial pressure	$\bar{\sigma}$: Equivalent of the von Mises' stress
p_H	: Hugoniot pressure		
s	: Material parameter		
s_1	: Shock EOS linear parameter S1		
s_2	: Shock EOS quadratic parameter S2		
t	: Time		

1. INTRODUCTION

There are many published studies¹⁻¹⁹ concerning FEM numerical models of a projectile impact on a target. Fang and Zhang¹ described a finite element analysis approach by which to investigate the impacts of projectiles on rock-rubble overlays, focusing on the accidentally of the structure. Another study by Kędzierski², *et al.* concerns the capabilities of five different numerical approaches, namely, FEM, FEM-

remeshing, ALE-smoothing, ALE-Euler, and SPH, and focuses on 9 mm Parabellum deformable projectiles. Other studies by Bresciani³, *et al.* present an approach for the Lagrangian finite element modelling of the fragmentation of a tungsten heavy-alloy blunt-shaped projectile penetrating a ceramic alumina tile. A paper written by Myagkov⁴, *et al.* contains experimental and numerical research on the impact of polyethylene and aluminium projectile sonstring and mesh bumpers at high velocities. Żochowski⁵, *et al.* describes numerical and experimental approaches of human bone failure mechanisms during projectile impacts. The authors of numerous studies⁶⁻⁸ use FEM to determine the protective abilities of personal armour, armour for vehicles (e.g., Kurtaran⁹, *et al.*), and general use armour¹⁰⁻¹³. Fras¹⁴ described an investigation that thoroughly examined the influence of the initial pitch and yaw angles on the after-perforation of a 7.62 mm×51 AP P80 projectile's performance.

There are a few available works¹⁵⁻²¹ on similar topics, and these works include considerations of the influences of the impact angles of different types of projectiles on terminal ballistics parameters. A study conducted by Weiss¹⁵, *et al.* focuses on the ricochets caused by a 25 mm APDS-T projectile. Three different hardness armour steel plates were impacted at varying angles of incidence. The main conclusion was that the ricochet angle decreased with an increase in target hardness. Goldsmith¹⁶, *et al.* describes investigations of targets subjected to non-standard collisions that involve different impact angles. Ansari¹⁷, *et al.* conducted experimental and FEM analyses of the perforation of unidirectional glass fibre-reinforced cross-ply laminates, considering different projectile nose shapes, incidence velocities, incidence angles, and laminate thicknesses. The influences of the projectile shape and impact angle on the ballistic limit, failure mechanism, and ricochet angle were studied by Iqbal¹⁸, *et al.* Luo¹⁹, *et al.* examined the effect of high-rate dynamic comminution on the penetration of projectiles with different velocities and impact angles into concrete. Lamontagne²⁰, *et al.* tested the effects of projectile density, impact angle and energy on the damage caused by hypervelocity impacts (2.71–7.14 km/s) on carbon fibre/PEEK composites. The aforementioned literature¹⁶⁻²⁰ mainly concerns the analysis of penetrators that are not in use; they are only experimental models. The present work focuses on a 5.56×45 mm SS109 military bullet in use. It is a full metal jacket bullet with a steel core placed in the front and a lead core located in the rear. In cases of ricochets, such double-core projectiles can act differently from standard (single-core) bullets, as described by Muster²¹, *et al.*

This study focuses on numerical and experimental research on the impact of projectiles on an armour plate. The numerical approach provides more detailed information on this phenomenon, thereby enabling the determination of the velocity and energy in all axes of the projectile or its debris after impact. The analysis of this phenomenon using only a high-speed camera was limited, as it was not possible to accurately determine the projectile parameters, particularly the projectile particles. However, experimental tests allow for the validation of a numerical model based mainly on traces after impact on an armour plate.

The following analysis determines the influence of the impact angle on the armour protection capability and effects of this impact. This information is important during the development process of newly designed vehicles or personal armours.

2. NUMERICAL MODEL

2.1 Mathematical Description of Numerical Model

An (equation of state) linear material model was used for the steel core of the projectile and armour plate. This model defines a linear equation of state using the bulk modulus, which is characterised by the following Eqn.²².

$$K = -V \frac{dp}{dV} \quad (1)$$

Shock equations of state (EOS) linear material models were adopted for the Tombac jacket and lead core of the projectile. This model describes the dependence of shock velocity and particle velocity using the following Eqn.²²⁻²⁵.

$$u_s = c_0 + s_1 u_p + s_2 u_p^2 \quad (2)$$

The Mie-Grüneisen form of the state equation based on Hugoniot shock was used. This is described by the following formula²²⁻²⁵,

$$p = p_H + \Gamma \rho (e - e_H) \quad (3)$$

where, it is assumed to follow the following formula²²⁻²⁵.

$$\Gamma \rho = \Gamma_0 \rho_0 = \text{const.} \quad (4)$$

The Hugoniot pressure and internal energy per unit mass can be calculated the following equation²²⁻²⁵.

$$p_H = \frac{p_0 c_0^2 \left(1 - \frac{V}{V_0}\right)}{\left[1 - s \left(1 - \frac{V}{V_0}\right)\right]^2} \quad (5)$$

$$e_H = \frac{1}{2} p_H (V_0 - V) \quad (6)$$

Table 1 includes the material data adopted for the EOS linear model and shock EOS linear model.

Table 1. Material parameters for the equations of state²⁵

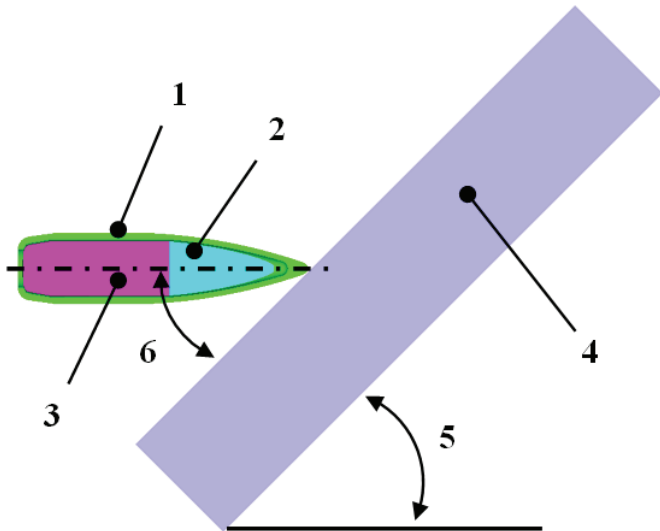
Material	EOS linear model			
	K (GPa)			
Steel (core)	172.5			
Armox 600 armour steel	172.5			
Shock EOS linear model				
	Γ	c_0 (m/s)	S_1	S_2
Tombac	2.04	3726	1.434	0
Lead	2	2092	1.452	0

The Johnson-Cook strength model was used in the study. This model contains the stresses, strains, strain rates, and temperature distribution in the material and was adopted for the Tombac jacket, steel core, and steel armour plate. This is described by the following Eqn.^{6,22-23,25-26}.

$$\sigma = [A + B \varepsilon^n] \times [1 + C \ln \dot{\varepsilon}^*] \times [1 - T^{*m}] \quad (7)$$

Table 2. Material data used in the numerical models^{6,25-27}

Material	Johnson–cook strength model					Johnson–cook failure model				
	A (GPa)	B (GPa)	C	n	m	D ₁	D ₂	D ₃	D ₄	D ₅
Steel (core)	0.792	0.51	0.014	0.26	1.03	0.05	3.44	-2.12	0.002	0.61
Tombac	0.112	0.505	0.009	0.42	1.68	0.54	4.89	3.03	0.014	1.12
Armox 600 armour steel	1.58	0.958	0.00877	0.175	0.712	-0.4	1.5	-0.5	0	0
Von Mises Strength Model										
	Y(MPa)					G(GPa)				
Lead	30					11.13				



The dimensionless plastic strain rate and homologous temperature, which are dimensionless temperature values, can be calculated using the following Eqn.^{6,22-23, 25}.

$$\dot{\epsilon}^* = \frac{\epsilon}{\epsilon_0} \tag{8}$$

$$T^* = \frac{T - T_p}{T_i - T_p} \tag{9}$$

The Johnson-Cook failure model was adopted for the Tombac jacket, steel core, and steel armour plate. This model determines deformation at failure using the following Eqn.^{6,22-23,25}.

$$\epsilon^f = [D_1 + D_2 e^{D_3 \sigma^*}] \times [1 + D_4 \ln(\dot{\epsilon}^*)] \times [1 + D_5 T^*] \tag{10}$$

The pressure/stress measureless dependence can be calculated the following Eqn.^{6,22-23, 25}

Figure 1. Numerical model. 1, 2, 3—parts of the 5.56×45 mm SS109 projectile;1—tombac jacket; 2—steel core; 3—lead core; 4—Armox 600 armour plate;5—elevation angle of the plate; 6—impact angle of projectile.

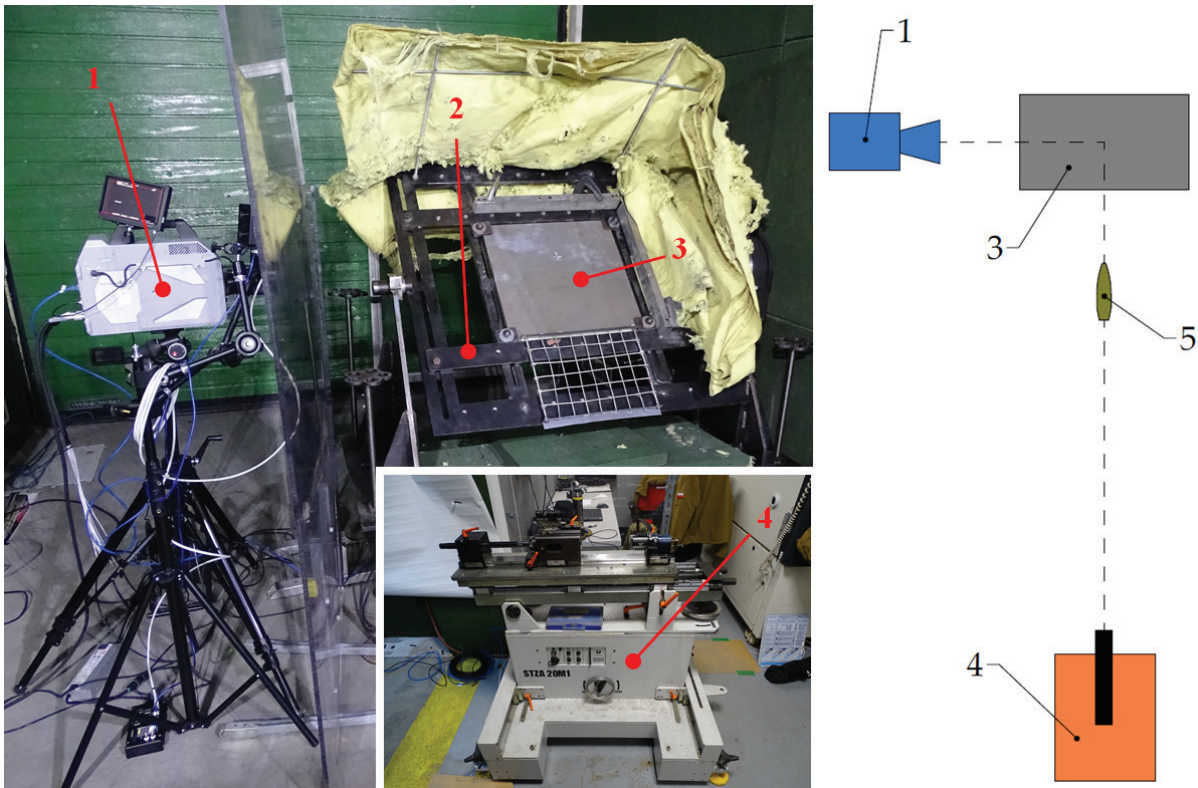

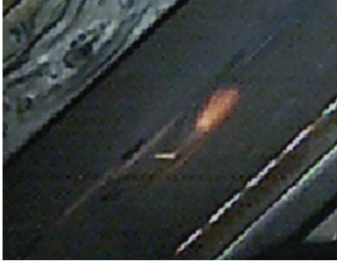

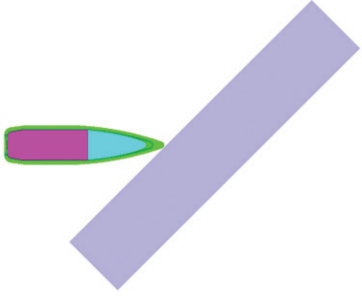
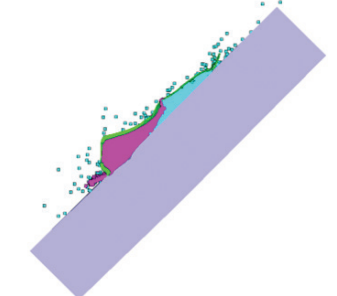
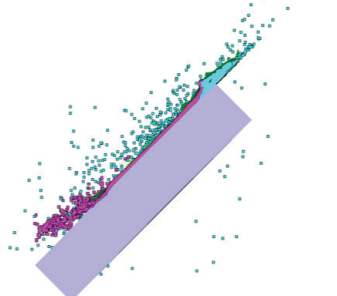
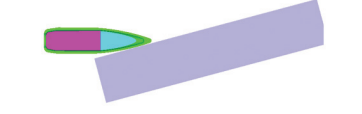
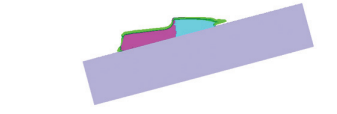
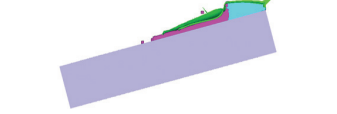
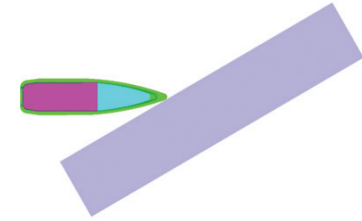
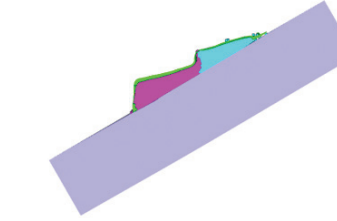
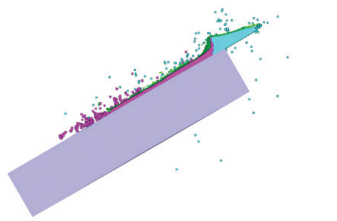
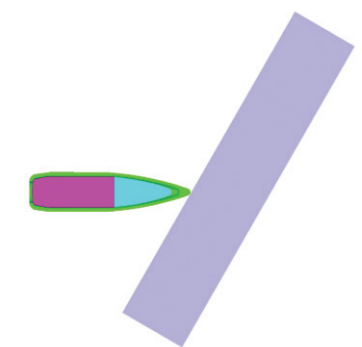
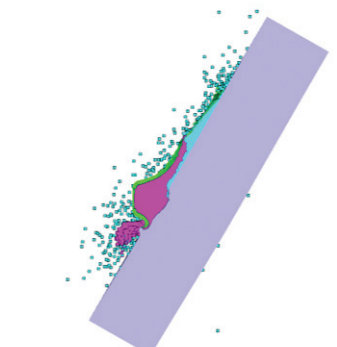
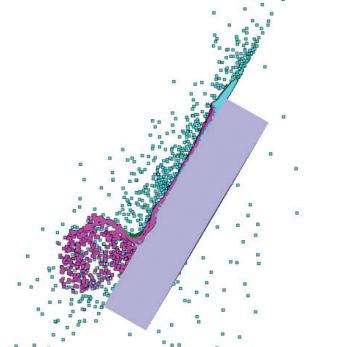
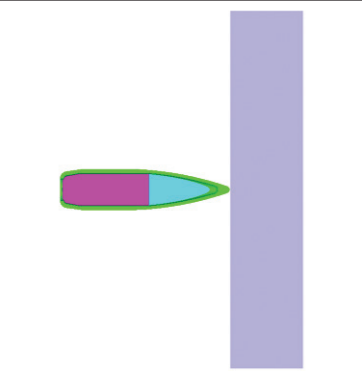
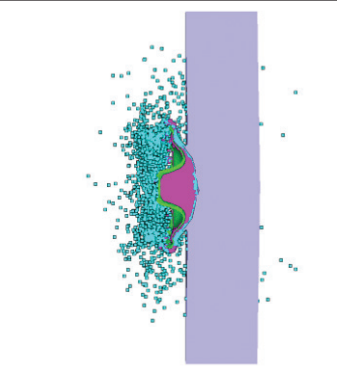
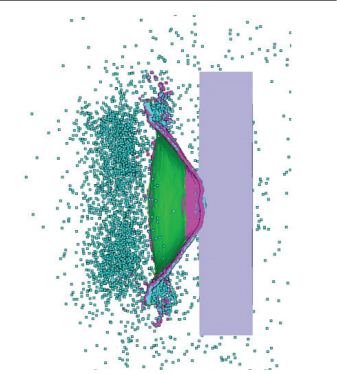


Figure 2. Laboratory stand used during the tests. 1—Photron fastcam SA-Z 2100K high-speed camera; 2—mounting stand for plates; 3—Armox 600 armour plate; 4—ballistic mount and ballistic barrel; 5—projectile.

Table 3. Comparison of the high-speed camera frames and FEM simulation

t (μ s)	$t_0 = 0$	$t_1 = 20$	$t_2 = 40$
High-speed camera frames 45°			
Simulation 45°			
Simulation 15°			
Simulation 30°			
Simulation 60°			
Simulation 90°			

$$\sigma^* = \frac{p}{\bar{\sigma}} \tag{11}$$

When the parameter D is equal to 1, a failure occurs^{6,22-23, 25}.

$$D = \sum \frac{\Delta \epsilon}{\epsilon^f} \tag{12}$$

The von Mises strength model was used for the projectile lead cores. The model assumes that the yield stress and shear modulus have constant values^{23, 25}.

Table 2 lists the material data used in the Johnson–Cook strength, Johnson–Cook failure, and von Mises strength models.

2.2 Development of Numerical Model

The FEM numerical model (Fig. 1) was developed using ANSYS Autodyn software. The projectile impact velocity was set at 987 m/s, which is the value that was measured in the experiment. The Armox 600 armour plate was fixed on four

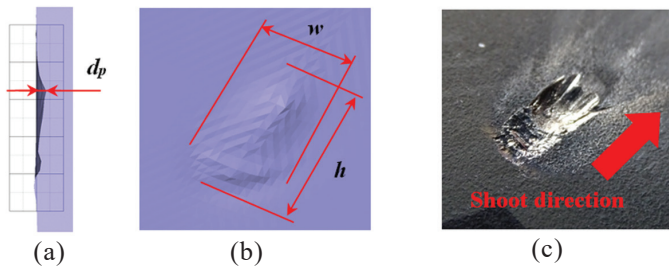


Figure 3. Comparison of the traces from the FEM simulation and experiment for a projectile impact angle of 45°.

side surfaces with a thickness of 10 mm, as in the experiment. The elevation angle of the armour plate was set equal to the impact angle of the projectile on the plate.

3. EXPERIMENTAL TESTS

The laboratory stand used for the experimental tests (Fig. 2) consisted of a Photron Fastcam SA-Z 2100 K high-speed camera, mounting stand with a 500 mm × 500 mm × 10 mm Armox 600 armour plate, and ballistic mount with a 5.56×45 mm ballistic barrel. The recording speed of the high-speed camera was 50,400 frames per second (fps), the ammunition used in the experiment was 5.56×45 mm HC (SS109) Ruag, the projectile weight was 4.0 g²⁸, the projectile impact velocity was 987 m/s, and the projectile impact energy was 1948 J (the last two values measured during the experiment).

4. RESULTS AND VALIDATION OF THE NUMERICAL MODEL

The high-speed camera frames and FEM simulation presented in Table 3 compare the course of the phenomenon for the times of 0 μs, 20 μs and 40 μs. Table 3 shows a comparison of the numerical simulation results for different impact angles of the projectile (elevation angle of the armour plate): 15°, 30°, 45°, 60°, and 90°. The time of 0 μs corresponds to the beginning of the impact.

The most important factor for the validation of the numerical model is the comparison of the traces on the armour plate from the numerical investigation and experiment. Figure 3 and Table 4 show the qualitative and quantitative

Table 4. Comparison of the trace parameters obtained experimentally and via a numerical approach

Parameters of the trace	h (mm)	w (mm)	d_p (mm)
Numerical investigation, 45°	7.4	5.4	0.44
Experimental test, 45°	9.7	4.8	0.35
Difference compared with the experiment	-2.3	+0.6	+0.09
Relative difference, %	-23.7	+12.5	+25.7
Numerical investigation, 15°	0	0	0
Numerical investigation, 30°	5.6	6.3	0.25
Numerical investigation, 60°	7.55	5.6	1.18
Numerical investigation, 90°	12.09	12.22	1.61

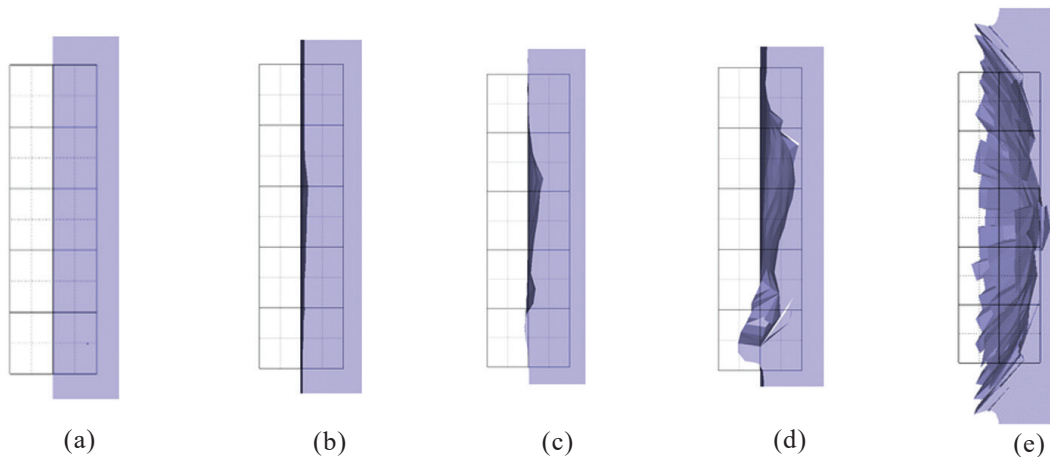


Figure 4. Comparison of the traces from the FEM simulations for various projectile impact angles.

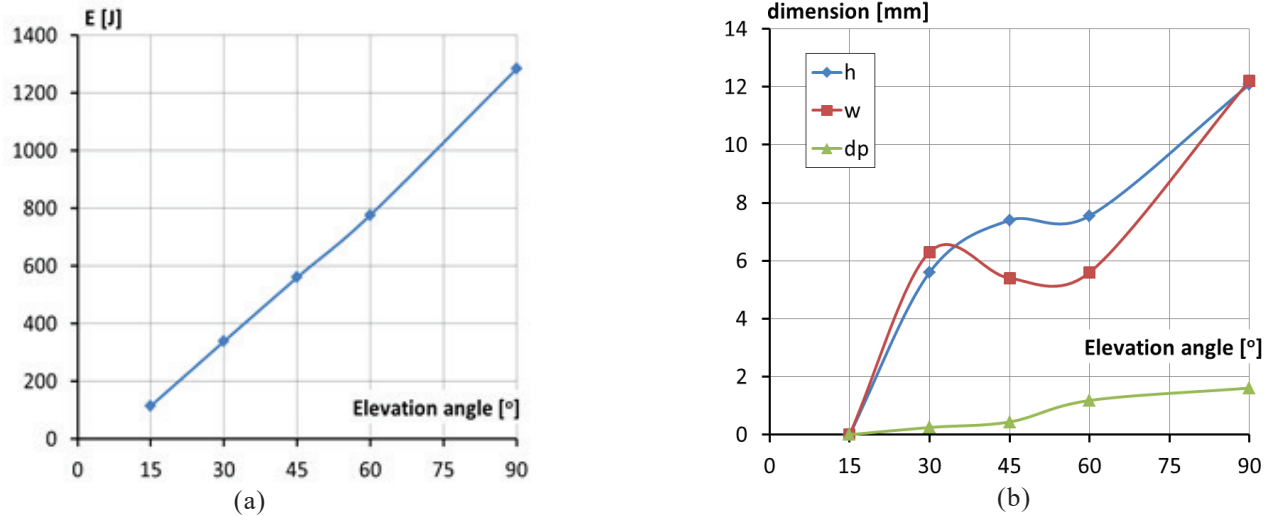


Figure 5. (a) Energy transferred into the armour plate versus projectile impact angle. (b) Trace dimensions (height, width, and penetration depth) versus projectile impact angle.

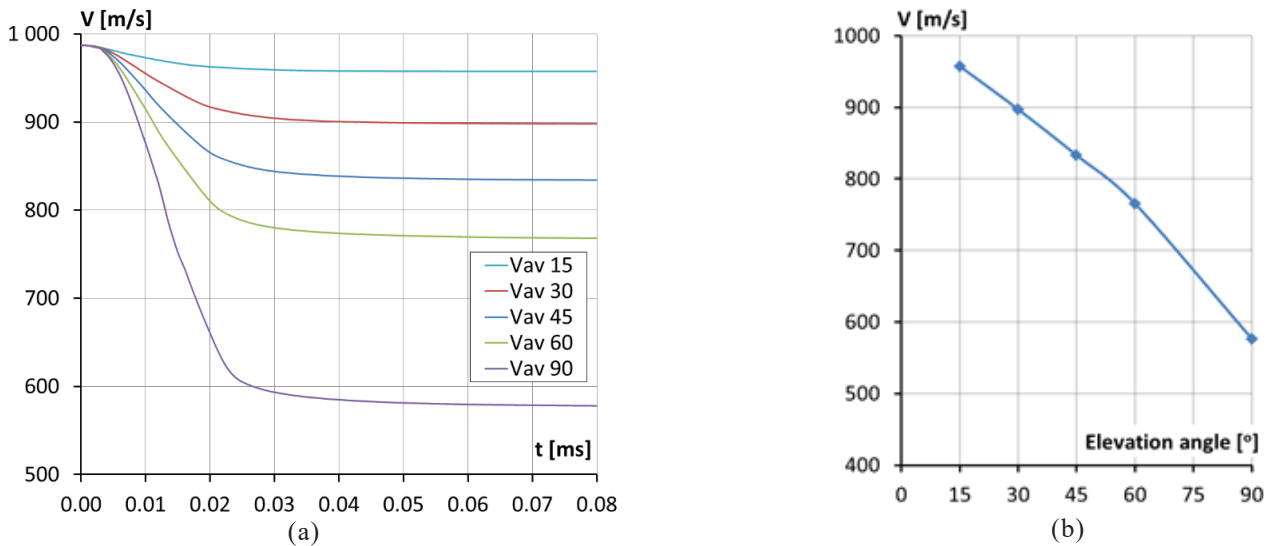


Figure 6. Influence of the projectile impact angle on the average velocity of projectile debris. (a) Average velocity of projectile debris versus time. (b) Average velocity of projectile debris ($t = 0.08$ ms) versus projectile impact angle.

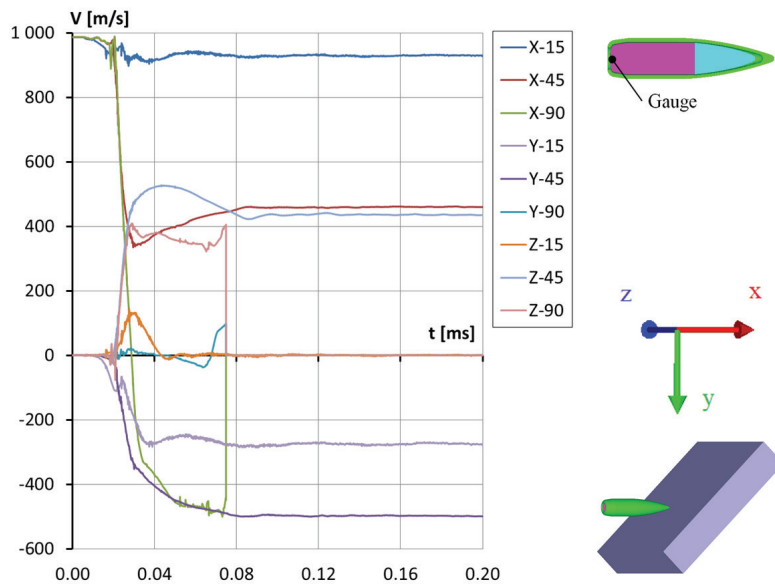


Figure 7. Influence of the projectile impact angle on the gauge velocity along different axes.

similarities between the traces obtained using both the experiment and FEM investigation for a 45° projectile impact angle.

Figure 4 shows the traces on the armour plate after the impact of the projectile at different impact angles. Table 4 lists the trace dimensions for these angles. The largest difference is noticeable for the traces for impact angles of 15° and 90° because there is an 11 times difference in the energy transferred to the armour plate (Fig. 5a). The energy transferred to the plate corresponded to the energy loss of the projectile, which can be described as follows.

$$E_T = E_{k0} - E_{kr} \quad (13)$$

Figure 5(b) shows the dependence between the trace dimensions and projectile impact angle. Figure 6 shows the decrease in the average velocity of the projectile debris after impact with the armour plate.

Figure 7 shows the velocities of the gauge located in the rear part of the projectile along different axes.

5. DISCUSSION

A comparison of the traces obtained from the numerical investigation and experimental tests (Fig. 3, Table 4) revealed qualitative and quantitative similarities, thereby proving the accuracy of the numerical model. The developed numerical model accurately describes the real phenomenon of a projectile impacting an armour plate. This analysis allowed us to closely investigate the phenomenon of armour plate degradation during projectile impact. It was possible to determine the average speed of the projectile particles and their speeds in different directions (OX, OY, and OZ axes). This study also determined the projectile temperature during impact and estimated the fire hazard from a ricocheting projectile, as described by Badurowicz²⁹, *et al.* Additionally, this type of analysis can be used for research on new armour systems or to improve existing ones, such as those composed of new materials or composite structures.

6. CONCLUSIONS

After carrying out the above investigations, the following conclusions can be drawn.

- The highest deformation of the armour plate occurred for a 90° projectile impact angle (Table 4, Fig. 4). This occurs because the amount of energy transferred to the armour plate increases with an increase in the projectile impact angle (in the range of 0–90°)
- The dependence of the energy transferred to the armour plate and the decrease in the average velocity of the projectile debris as a function of the projectile impact angle were almost linear (Fig. 5(a), Fig. 6(b))
- The transfer of energy into the armour plate is strictly related to the dimensions of the traces after impact. As the energy increased, the dimensions of the traces increased (Fig. 5(b))
- The largest decrease in the average velocity of the projectile debris occurs for a projectile impact angle of 90° (Fig. 6)
- The greatest decrease in velocity along the OX axis occurs for a projectile impact angle of 90°, and the greatest

increase in velocity along the OY and OZ axes occurs for a projectile impact angle of 45° (Fig. 7)

- The protection capability of an armour plate increases when the projectile impact angle decreases (in the range of 0–90°).

REFERENCES

1. Fang, Q. & Zhang, J. 3D numerical modelling of projectile penetration into rock-rubble overlays accounting for random distribution of rock-rubble. *Int. J. Impact Eng.*, 2014, **63**, 118-128. doi: 10.1016/j.ijimpeng.2013.08.010
2. Kędzierski P.; Morka, A.; Stanisławek S. & Surma, Z. Numerical modelling of the large strain problem in the case of mushrooming projectiles. *Int. J. Impact Eng.*, 2020, **135**. doi: 10.1016/j.ijimpeng.2019.103403
3. Bresciani, L.M.; Manes, A.; Romano, T.A.; Iavarone, P. & Giglio, M. Numerical modelling to reproduce fragmentation of a tungsten heavy alloy projectile impacting a ceramic tile: Adaptive solid mesh to the SPH technique and the cohesive law. *Int. J. Impact Eng.*, 2016, **87**, 3-13. doi: 10.1016/j.ijimpeng.2015.10.003
4. Myagkov, N.N.; Shumikhin, T.A. & Bezrukov, L.N. Experimental and numerical study of peculiarities at high-velocity interaction between a projectile and discrete bumpers. *Int. J. Impact Eng.*, 2010, **37**, 980-994.
5. Żochowski, P.; Cegła, M.; Berent, J.; Grygoruk, R.; Szlązak, K. & Smędra, A. Experimental and numerical study on failure mechanisms of bone simulants subjected to projectile impact. *Int. J. Num. Methods in Biomed. Eng.*, 2023. doi: 10.1002/cnm.3687
6. Wiśniewski, A. & Pacek, D. Flexible modular armour for protection against the 5.56×45 mm SS109 projectiles. *Problems of Mechatronic.: Arm., Aviation, Safety Eng.*, 2015, **6**, 21-40. doi: 10.5604/20815891.1157772
7. Pyka, D.; Jamroziak, K.; Blazejewski, W. & Bocian, M. Calculations with the Finite Element Method During the design ballistic armour. In Rusiński, E., Pietrusiak, D. (eds) Proceedings of the 13th International Scientific Conference, RESRB 2016. Lecture Notes in Mechanical Engineering. Springer, Cham, 2017. doi: 10.1007/978-3-319-50938-9_47
8. Zochowski, P.; Bajkowski, M.; Grygoruk, R.; Magier, M.; Burian, W.; Pyka, D.; Bocian, M. & Jamroziak, K. Finite element modelling of ballistic inserts containing aramid fabrics under projectile impact conditions – Comparison of methods. *Composite Structures*, 2022, **294**(4):115752. doi: 10.1016/j.compstruct.2022.115752
9. Kurtaran, H.; Buyuk, M. & Eskandarian, A. Ballistic impact simulation of GT model vehicle door using finite element method. *Theoretical and Appl. Fracture Mechanic.*, 2003, **40**(2), 113-121. doi: 10.1016/S0167-8442(03)00039-9
10. Feli, S. & Asgari, M.R. Finite element simulation of ceramic/composite armor under ballistic impact. *Composites Part B: Eng.*, 2011, **42**(4), 771-780.

11. Zukas, J.A. & Scheffler, D.R. Impact effects in multilayered plates. *Int. J. Solids and Struct.*, 2021, **38**, 3321-3328.
12. Mahfuz, H.; Zhu, Y.; Haque, A.; Abutalib, A.; Vaidya, U.; Jeelani, S.; Gama, B.; Gillespie, J. & Fink, B. Investigation of high-velocity impact on integral armor using finite element method. *Int. J. Impact Eng.*, 2000, **24**, 203-217.
13. Børvik, T.; Hopperstada, O.S.; Berstadb, T. & Langseth M. Perforation of 12 mm thick steel plates by 20 mm diameter projectiles with flat, hemispherical and conical noses: Part II: numerical simulations. *Int. J. Impact Eng.*, 2022, **27**, 37-64.
14. Fras, T. On the effect of pitch and yaw angles in oblique impacts of small-caliber projectiles. *Defence Technol.*, 2024, **31**, 73-94.
doi: 10.1016/j.dt.2023.06.004
15. Weiss, A.; Borenstein, A.; Paris, V.; Ravid, M. & Shapira N. Evaluation of critical ricochet angles for 25 mm APDS-T projectile on metallic targets - Modeling and verification. Proceedings of the 2019 Hypervelocity Impact Symposium, 2019, **HVIS2019**, 82-88.
16. Goldsmith, W. Non-ideal projectile impact on targets. *Int. J. Impact Eng.*, 1999, **22**(2-3), 95-395.
doi: 10.1016/S0734-743X(98)00031-1
17. Ansari, Md. M. & Chakrabarti, A. Influence of projectile nose shape and incidence angle on the ballistic perforation of laminated glass fiber composite plate. *Composites Sci. Technol.*, 2017, **142**, 107-116.
doi: 10.1016/j.compscitech.2016.12.033
18. Iqbal, M.A.; Diwakar, A.; Rajput, A. & Gupta, N.K. Influence of projectile shape and incidence angle on the ballistic limit and failure mechanism of thick steel plates. *Theoretical and Appl. Fracture Mech.*, 2012, **62**, 40-53.
doi: 10.1016/j.tafmec.2013.01.005
19. Luo, W.; Chau, V.T. & Bažant, Z.P. Effect of high-rate dynamic comminution on penetration of projectiles of various velocities and impact angles into concrete. *Int. J. Fracture*, 2019, **216**, 211-221.
doi: 10.1007/s10704-019-00354-0
20. Lamontagne, Ch. G.; Manuelpillai, G.N.; Kerr, J.H.; Taylor, E.A.; Tennyson, R.C. & Burchell, M.J. Projectile density, impact angle and energy effects on hypervelocity impact damage to carbon fibre/peek composites. *Int. J. Impact Eng.*, 2001, **26**(1-10), 381-398.
doi: 10.1016/S0734-743X(01)00110-5
21. Muster, M.; Hameed, A. & Wood, D. Ricochet quantification using a multiple sensor approach. *Defence Technol.*, 2021, **17**, 305-3314.
doi: 10.1016/j.dt.2020.02.017.
22. ANSYS Theory Reference, 001242, 11th edition, SAS IP, Inc.
23. Ansys help. <https://www.ansyshelp.ansys.com/> (Accessed on 9 March 2023).
24. Yang, L.; Wang, H.; Chi, M.; Zeng, X.; Wang, Y. & Zhao, P. Molecular dynamics study on Hugoniot State and Mie-Grüneisen equation of state of 316 stainless steel for hydrogen storage tank, *Materials*, 2023, **16**, 628.
doi: 10.3390/ma16020628
25. Pacek, D. Shear thickening fluids and magnetorheological fluids in armours (in Polish). Military Institute of Armament Technology, 2018.
26. Johnson, G. & Cook, W. A constitutive model and data for metals subjected to large strains, high strain rates and high temperatures. In Proceedings of the 7th International Symposium on Ballistics, 1983, 541-547.
27. Nilsson, M. Constitutive model for ArmoX 500T and ArmoX 600T at low and medium strain rates. Technical Report, Swedish Defence Research Agency, Tumba, Sweden, 2003.
28. Website of RUAG Company. [https://www.parnisariarms.com/userdata/cataloghi/MUNIZIONI/RUAG/4030_5.56x45_HC_\(SS109\)_4.0_g_-_62_gr_EN.pdf](https://www.parnisariarms.com/userdata/cataloghi/MUNIZIONI/RUAG/4030_5.56x45_HC_(SS109)_4.0_g_-_62_gr_EN.pdf) (Accessed on 23 March 2023).
29. Badurowicz, P. & Pacek, D. Determining ricocheting projectiles' temperature using numerical and experimental approaches, *Materials*, 2022, **15**, 928.
doi: 10.3390/ma15030928

ACKNOWLEDGEMENT

The National Centre for Research and Development (financing agreement number: DOB-BIO10/11/02/2019)

CONTRIBUTORS

Dr Przemysław Badurowicz is an Assistant Professor at the Ballistic Department of the Military Institute of Armament Technology in Zielonka, Poland. He obtained his PhD in the specialty design and research of firearms at the Military University of Technology in Warsaw, Poland. His main area of research is small arms, small arms ammunition, ballistics, and numerical methods.

Contributions in current study is conceptualisation, methodology, software, validation, formal analysis, investigation, resources, data curation, writing, original draft preparation and visualisation.

Mr Dawid Pacek is an Assistant Professor at the Military Institute of Armament Technology in Zielonka, Poland. His scientific activity has mainly focused on issues related to the impact of projectile energy and white weapons on armour. He has designed shields, tested their protective ability, and simulated the process of armour perforation using numerical methods. Contributions to the current study is conceptualisation, methodology, software, validation, formal analysis, investigation, resources, data curation, writing - original draft preparation, and visualisation.